Tang *et al.*
Protection and Control of Modern Power Systems (2023) 8:44
https://doi.org/10.1186/s41601-023-00318-6

Protection and Control of
Modern Power Systems

ORIGINAL RESEARCH

Open Access

Fault location of untransposed double-circuit transmission lines based on an improved Karrenbauer matrix and the QPSO algorithm

Minan Tang[1*], Hang Lu[1] and Bin Li[2]

Abstract

Some double-circuit transmission lines are untransposed, which results in complex coupling relations between the parameters of the transmission lines. If the traditional modal transformation matrix is directly used to decouple the parameters, it can lead to large errors in the decoupled modal parameter, errors which will be amplified in the fault location equation. Consequently, it makes the fault location results of the untransposed double-circuit transmission lines less accurate. Therefore, a new modal transformation method is needed to decouple the parameter matrix of untransposed double-circuit transmission lines and realize the fault location according to the decoupled modal parameter. By improving the basis of the Karrenbauer matrix, a modal transformation matrix suitable for decoupling parameters of untransposed double-circuit transmission lines is obtained. To address the difficulties in solving the fault location equation of untransposed double-circuit transmission lines, a new fault location method based on an improved Karrenbauer matrix and the quantum-behaved particle swarm optimization (QPSO) algorithm is proposed. Firstly, the line parameter matrix is decomposed into identical and inverse sequence components using the identical-inverse sequence component transformation. The Karrenbauer matrix is then transformed to obtain the improved Karrenbauer matrix for untransposed double-circuit transmission lines and applied to identical and inverse sequence components to solve the decoupled modal parameter. Secondly, based on the principle that voltage magnitudes at both ends are equal, the fault location equation is expressed using sequence components at each end, and the QPSO algorithm is introduced to solve the equation. Finally, the feasibility and accuracy of the proposed method are verified by PSCAD simulation. The simulation results fully demonstrate that the innovative improvement on the basis of the traditional modal transformation matrix in this paper can realize the modal transformation of the complex coupling parameters of the untransposed double-circuit transmission lines. It causes almost no errors in the decoupling process. The QPSO algorithm can also solve the fault location equation more accurately. The new fault location method can realize the accurate fault location of untransposed double-circuit transmission lines.

Keywords Fault location, Untransposed double-circuit transmission lines, Karrenbauer matrix, Quantum particle swarm optimization, Modal transformation

*Correspondence:
Minan Tang
tangminan@mail.lzjtu.cn
Full list of author information is available at the end of the article

1 Introduction

Double-circuit and multi-circuit transmission lines are widely used [1, 2]. In principle, transposition measures are adopted for high-voltage transmission lines to reduce the asymmetric three-phase parameters. However, in the actual construction of transmission lines, there is no condition for some lines to adopt complete transposition [3, 4]. The asymmetric three-phase parameters caused by untransposition affect the accuracy of fault location [5]. Therefore, research on fault location method for untransposed double-circuit transmission lines is relevant to engineering practice [6, 7]. As an important means for eliminating parameter coupling between lines and phases, modal transformation is the basis of fault location. For completely transposed double-circuit transmission lines, the six sequence components method [8] decomposes them into the identical and inverse components, eliminates the mutual inductances between lines, and realizes parameter decoupling.

For untransposed double-circuit transmission lines, the parameters of a single circuit line itself or between two circuits are no longer symmetrical, so the Fortescue's transformation method and six sequence components method are no longer applicable. There are two methods for parameter decoupling of untransposed transmission lines, i.e., phase component and modulus component methods. The phase component method is intuitive and its physical meaning is clear, but the calculation process is relatively complex and the amount of calculation is large. In [9], the phase component method is used for modeling, and for the parameter asymmetry caused by untransposition, the mutual inductance matrix elements are adjusted for balance. In [10], the phase component model is improved and the polymorphic phase component method is proposed to solve the problem of parameter asymmetry. In [11], matrix diagonalization transformation is used to improve the phase component method and reduce the amount of calculation of the phase component method. In [12], the symmetry of two side conductors are used to calculate impedance and admittance matrices of the line in the phase domain.

The key to the module component method is to find an appropriate transformation matrix to realize the transformation from phasor to modulus. In [13], a transformation matrix based on the Clark matrix is proposed, but it is only applicable to single-circuit lines without transposition and cannot solve the coupling problem in double-circuit transmission lines. In [14], the zero order approximation method is proposed to deal with the asymmetry of line parameters by obtaining the average approximation, whereas in [15], the existing transformation matrix is improved and a first-order disturbance theory is put forward, but it is also only applicable to untransposed single-circuit lines.

With the development of intelligent algorithms, transmission line fault location equations are being more and more optimized by the PSO [16], ant colony [17], and genetic algorithms [18], and neural networks [19, 20], etc. However, these algorithms have problems such as too many iterations and find it easy to fall into local optima. Compared with these algorithms, the quantum-behaved particle swarm optimization (QPSO) has fewer parameters [21] and is easier to implement. In theory, it has global optimal convergence [22], and can converge to the global best and avoid the local best.

In this paper, the traditional modal transformation matrix is improved, so that the improved Karenbauer matrix can be applied to the decoupling of complex coupling parameters of untransposed double-circuit transmission lines. The quantum particle swarm optimization algorithm is introduced to propose a new fault location method suitable for untransposed double-circuit transmission lines. The main contributions of this paper are as follows: first, the structural characteristics and parameter coupling of untransposed double-circuit transmission lines are analyzed, and their coupling parameter model is established. To solve the problem that the parameter coupling of untransposed double-circuit transmission lines is complicated and the traditional modal transformation matrix is no longer applicable, the standard Karenbauer matrix is then transformed according to the coupling relation, and the line parameter matrix is decomposed into identical and inverse sequence components. By combining the transformed Karenbauer matrix with the identical-inverse sequence component transformation matrix, an improved Karenbauer matrix suitable for modal transformation of untransposed double-circuit transmission lines is obtained. Finally, based on the even transmission line equation, the fault location equation of untransposed double-circuit transmission lines is established. There is a problem in that the location equation is a transcendental equation composed of hyperbolic functions with multi-dimensional complex variables and there is no exact analytical solution. Thus the quantum particle swarm optimization algorithm with global searching ability and higher iterative efficiency is introduced to optimize the equation. A new fault location method for untransposed double-circuit transmission lines is then obtained.

2 Solution of improved Karrenbauer matrix and parameter modal transformation

2.1 Parameter matrix

The model of untransposed double-circuit transmission lines is shown in Fig. 1, where p and q represent

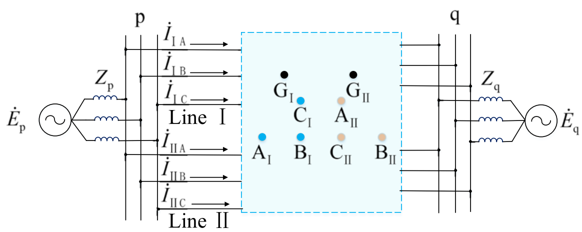

Fig. 1 Model of untransposed double-circuit transmission lines

the sender and receiver of the system, respectively. $\dot{E}_p$ and $\dot{E}_q$ are the EMF of the power supply at the sending end and the receiving end respectively, whereas Z_p and Z_q are the source impedances of the sender and the receiver, respectively.

Taking the line shown in Fig. 1 as an example, the form of impedance and admittance matrices for the double-circuit lines can be obtained as:

$$Z=\begin{bmatrix} Z_{11} & Z_{12} & Z_{13} & Z_{14} & Z_{15} & Z_{16} \\ Z_{12} & Z_{22} & Z_{23} & Z_{15} & Z_{25} & Z_{26} \\ Z_{13} & Z_{23} & Z_{33} & Z_{16} & Z_{26} & Z_{36} \\ Z_{14} & Z_{15} & Z_{16} & Z_{11} & Z_{12} & Z_{13} \\ Z_{15} & Z_{25} & Z_{26} & Z_{12} & Z_{22} & Z_{23} \\ Z_{16} & Z_{26} & Z_{36} & Z_{13} & Z_{23} & Z_{33} \end{bmatrix} \tag{1}$$

$$Y=\begin{bmatrix} Y_{11} & Y_{12} & Y_{13} & Y_{14} & Y_{15} & Y_{16} \\ Y_{12} & Y_{22} & Y_{23} & Y_{15} & Y_{25} & Y_{26} \\ Y_{13} & Y_{23} & Y_{33} & Y_{16} & Y_{26} & Y_{36} \\ Y_{14} & Y_{15} & Y_{16} & Y_{11} & Y_{12} & Y_{13} \\ Y_{15} & Y_{25} & Y_{26} & Y_{12} & Y_{22} & Y_{23} \\ Y_{16} & Y_{26} & Y_{36} & Y_{13} & Y_{23} & Y_{33} \end{bmatrix} \tag{2}$$

where Z_{ii} is the self-impedance of the ith line, Z_{ij} is the mutual impedance between the ith and jth conductors.Y_{ii} is the self-admittance of the ith conductor, while Y_{ij} is the mutual admittance between the ith and jth conductors. $i=1,2,\ldots,6$ and $j=1,2,\ldots,6$.

For completely transposed double-circuit transmission lines, because of their high symmetry, the impedance matrix and the admittance matrix respectively satisfy:

$$\begin{cases} Z_{11}=Z_{22}=Z_{33} \\ Z_{12}=Z_{13}=Z_{23} \\ Z_{14}=Z_{15}=Z_{16}=Z_{25}=Z_{26}=Z_{36} \end{cases} \tag{3}$$

$$\begin{cases} Y_{11}=Y_{22}=Y_{33} \\ Y_{12}=Y_{13}=Y_{23} \\ Y_{14}=Y_{15}=Y_{16}=Y_{25}=Y_{26}=Y_{36} \end{cases} \tag{4}$$

The untransposition of double-circuit transmission lines is shown in Fig. 2. Theoretically, for the impedance and admittance matrices of untransposed double-circuit transmission lines, due to their high asymmetry, the elements in the matrices satisfy:

$$\begin{aligned} Z_{11}\neq Z_{22}\neq Z_{33}\neq Z_{12}\neq Z_{13}\neq Z_{23}\neq Z_{14} \\ \neq Z_{15}\neq Z_{16}\neq Z_{25}\neq Z_{26}\neq Z_{36} \end{aligned} \tag{5}$$

$$\begin{aligned} Y_{11}\neq Y_{22}\neq Y_{33}\neq Y_{12}\neq Y_{13}\neq Y_{23}\neq Y_{14} \\ \neq Y_{15}\neq Y_{16}\neq Y_{25}\neq Y_{26}\neq Y_{36} \end{aligned} \tag{6}$$

However, there is a certain degree of symmetry for the actual untransposed double-circuit transmission lines. Since in the relationship of conductor arrangement, conductors 1 and 3 are always symmetrical about conductor 2, while conductors 4 and 6 are always symmetrical about conductor 5, and thus, the impedance and admittance matrices of untransposed double-circuit transmission lines satisfy:

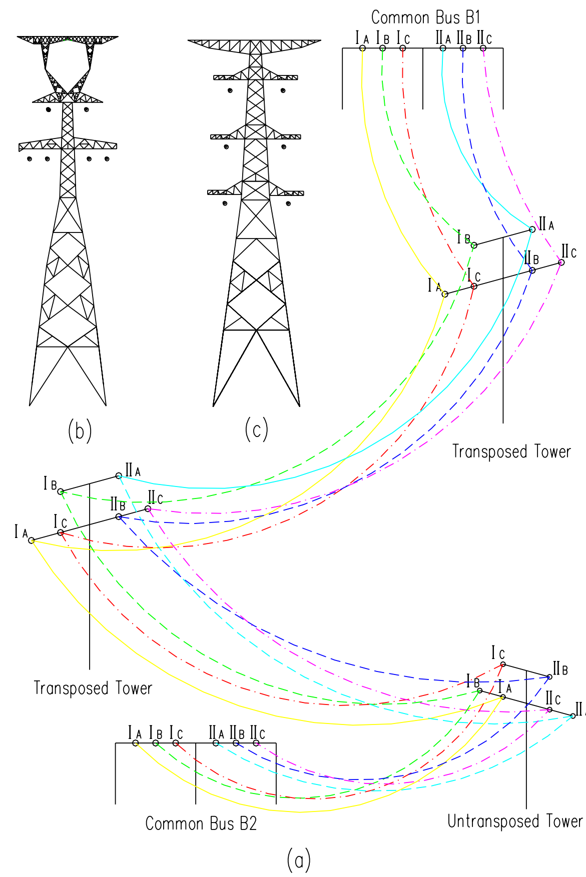

Fig. 2 Typical double-circuit transmission lines. **a** Conductor configuration of double-circuit lines, **b**, **c** different tower structure of double-circuit lines

$$\begin{cases} Z_{11} = Z_{33} \neq Z_{22} \\ Z_{12} = Z_{23} \neq Z_{13} \\ Z_{14} \neq Z_{15} \neq Z_{16} \neq Z_{25} \\ Z_{14} = Z_{36} \\ Z_{15} = Z_{26} \end{cases} \tag{7}$$

$$\begin{cases} Y_{11} = Y_{33} \neq Y_{22} \\ Y_{12} = Y_{23} \neq Y_{13} \\ Y_{14} \neq Y_{15} \neq Y_{16} \neq Y_{25} \\ Y_{14} = Y_{36} \\ Y_{15} = Y_{26} \end{cases} \tag{8}$$

For the impedance and admittance matrices satisfying (7) and (8), the six sequence components method [8] cannot be decoupled directly. Therefore, a new method based on improved Karrenbauer matrix is proposed to satisfy the modal transformation of the impedance and admittance matrices of untransposed double-circuit transmission lines.

2.2 Modal transformation

In this paper, two-terminal power frequency fault components are used for fault location. The location equation is based on the sinusoidal steady-state solution of the even transmission lines shown as:

$$\begin{cases} \frac{\mathrm{d}^2\boldsymbol{U}}{\mathrm{d}x^2} = \boldsymbol{ZYU} \\ \frac{\mathrm{d}^2\boldsymbol{I}}{\mathrm{d}x^2} = \boldsymbol{YZI} \end{cases} \tag{9}$$

where $\boldsymbol{U}$ is the voltage matrix, $\boldsymbol{I}$ is the current matrix, x is the line length, while $\boldsymbol{Z}$ and $\boldsymbol{Y}$ are the impedance and admittance matrices, respectively.

The matrices in (9) need to be decoupled, i.e., a suitable modal transformation matrix is selected to diagonalize the impedance and admittance product matrix $\boldsymbol{ZY}$, and the line parameters under phase measurement are transformed into a modulus. The transformation process is shown as:

$$\boldsymbol{T}^{-1}\boldsymbol{ZYT} = \boldsymbol{\lambda} \tag{10}$$

where $\boldsymbol{T}$ is the modal transformation matrix, $\boldsymbol{\lambda}$ is the eigenvalue matrix, a diagonal matrix, and each of its elements corresponds to a square of the propagation constant.

For completely transposed single-circuit transmission lines, common transformation matrices include Fortescue's, Clark's and Karrenbauer's, all of which can be used as decoupling of the equation in the modal transformation matrix in (9). However, the elements of the Karrenbauer's transformation matrix are real constants and do not change with frequency, so its structure is simpler and it is more widely used in practical calculation.

For double-circuit transmission lines, if they are transposed completely, the improved symmetrical component method, i.e., the six sequence components method, can be used to transform the impedance and admittance product $\boldsymbol{ZY}$. The modal transformation matrix is shown as:

$$\boldsymbol{S} = \boldsymbol{DP} = \begin{bmatrix} \boldsymbol{D} & \boldsymbol{D} \\ \boldsymbol{D} & -\boldsymbol{D} \end{bmatrix} \tag{11}$$

where $\boldsymbol{D} = \begin{bmatrix} 1 & \alpha & \alpha^2 \\ 1 & \alpha^2 & \alpha \\ 1 & 1 & 1 \end{bmatrix}$, $\boldsymbol{P} = \begin{bmatrix} \boldsymbol{I} & \boldsymbol{I} \\ \boldsymbol{I} & -\boldsymbol{I} \end{bmatrix}$, $\boldsymbol{I} = \begin{bmatrix} 1 & 0 & 0 \\ 0 & 1 & 0 \\ 0 & 0 & 1 \end{bmatrix}$, and $\alpha = \mathrm{e}^{\mathrm{j}120^\circ}$.

The matrix $\boldsymbol{D}$ in (11) is the standard Fortescue's transformation matrix, and matrix $\boldsymbol{P}$ as the identical and inverse transformation matrix can decompose the six phases of the double-circuit transmission lines into a group of the identical components and a group of inverse components. The combination of the two matrices constitutes the six sequence components transformation matrix. Because it is based on the Fortescue's transformation matrix, the six sequence components transformation matrix is not applicable to the modal transformation of untransposed double-circuit transmission lines. However, the identical and inverse transformation matrix $\boldsymbol{P}$ can still be applied in modal transformation of untransposed double-circuit transmission lines.

It should be pointed out that although $\boldsymbol{P}$ can still decompose the six phases of the untransposed double-circuit transmission lines, the decomposition does not result in the identical and inverse components in the strict sense. For convenience, the identical and inverse transformations are still used to describe untransposed double-circuit transmission lines in this paper, but the meanings are different from those of completely transposed double-circuit lines.

2.3 Solution of improved Karrenbauer matrix

For the impedance and admittance matrices of untransposed double-circuit transmission lines satisfying (7) and (8), the product matrix $\boldsymbol{ZY}$ is shown as:

$$\boldsymbol{ZY} = \begin{bmatrix} x & y & z & u & v & w \\ y & m & y & v & n & v \\ z & y & x & w & v & u \\ u & v & w & x & y & z \\ v & n & v & y & m & y \\ w & v & u & z & y & x \end{bmatrix} \tag{12}$$

where x, y, z, u, v, w, m, n represent the respective elements at the corresponding positions in the product matrix.

In order to obtain the improved Karrenbauer transformation matrix, matrix $\boldsymbol{P}$ can be used to decompose product matrix $\boldsymbol{ZY}$ into identical and inverse components, and obtain matrix $\boldsymbol{ZY}^{(1)}$ as:

$$\begin{aligned}\boldsymbol{ZY}^{(1)} &= \boldsymbol{P}^{-1}\boldsymbol{ZYP}\\ &= \begin{bmatrix} x+u & y+v & z+w & 0 & 0 & 0\\ y+v & m+n & y+v & 0 & 0 & 0\\ z+w & y+v & x+u & 0 & 0 & 0\\ 0 & 0 & 0 & x-u & y-v & z-w\\ 0 & 0 & 0 & y-v & m-n & y-v\\ 0 & 0 & 0 & z-w & y-v & x-u \end{bmatrix}\end{aligned} \tag{13}$$

Taking the standard Karrenbauer matrix applicable to single-circuit three-phase transmission lines in (11), it can be corrected to obtain matrix $\boldsymbol{K}'$ as:

$$\boldsymbol{K}' = \begin{bmatrix} 1 & 1 & 1 & 0 & 0 & 0\\ 1 & -2 & 1 & 0 & 0 & 0\\ 1 & 1 & -2 & 0 & 0 & 0\\ 0 & 0 & 0 & 1 & 1 & 1\\ 0 & 0 & 0 & 1 & -2 & 1\\ 0 & 0 & 0 & 1 & 1 & -2 \end{bmatrix} \tag{14}$$

Then, the matrix $\boldsymbol{K}'$ is used to transform matrix $\boldsymbol{ZY}^{(1)}$ to obtain matrix $\boldsymbol{ZY}^{(2)}$ as:

$$\begin{aligned}\boldsymbol{ZY}^{(2)} &= \boldsymbol{K}'^{-1}\boldsymbol{ZY}^{(1)}\boldsymbol{K}'\\ &= \boldsymbol{K}'^{-1}\boldsymbol{P}^{-1}\boldsymbol{ZYPK}'\\ &= \begin{bmatrix} a_{11} & a_{12} & a_{13} & 0 & 0 & 0\\ a_{21} & a_{22} & a_{23} & 0 & 0 & 0\\ 0 & 0 & a_{33} & 0 & 0 & 0\\ 0 & 0 & 0 & a_{44} & a_{45} & a_{46}\\ 0 & 0 & 0 & a_{54} & a_{55} & a_{56}\\ 0 & 0 & 0 & 0 & 0 & a_{66} \end{bmatrix}\end{aligned} \tag{15}$$

It can be seen from (15) that there is still coupling between components, so it is necessary to find a suitable matrix to diagonalize the matrix $\boldsymbol{ZY}^{(2)}$. First, the matrix $\boldsymbol{ZY}^{(2)}$ is partitioned to obtain the matrices $\boldsymbol{A}$ and $\boldsymbol{B}$ of the non-zero part of the matrix $\boldsymbol{ZY}^{(2)}$ as:

$$\boldsymbol{ZY}^{(2)} = \begin{bmatrix} \boldsymbol{A} & \boldsymbol{O}\\ \boldsymbol{O} & \boldsymbol{B} \end{bmatrix} \tag{16}$$

Then, the eigenvalue of matrix $\boldsymbol{A}$ is calculated as:

$$\begin{aligned}\boldsymbol{A} &= \det\begin{vmatrix} \lambda-a_{11} & -a_{12} & -a_{13}\\ -a_{21} & \lambda-a_{22} & -a_{23}\\ 0 & 0 & \lambda-a_{33} \end{vmatrix}\\ &= (\lambda-a_{33})\det\begin{vmatrix} \lambda-a_{11} & -a_{12}\\ -a_{21} & \lambda-a_{22} \end{vmatrix}\end{aligned} \tag{17}$$

The following characteristic values can be obtained:

$$\begin{cases} \lambda_{12} = \frac{a_{11}+a_{22}\pm\sqrt{(a_{11}-a_{22})^2+4a_{12}a_{21}}}{2}\\ \lambda_3 = a_{33} \end{cases} \tag{18}$$

where λ_1 takes $+$ and λ_2 take $-$.

The matrix consisting of the eigenvectors $\boldsymbol{S}_1, \boldsymbol{S}_2, \boldsymbol{S}_3$ corresponding to the eigenvalues $\lambda_1, \lambda_2, \lambda_3$ of matrix $\boldsymbol{A}$ are shown as:

$$\boldsymbol{S} = [\boldsymbol{S}_1, \boldsymbol{S}_2, \boldsymbol{S}_3] = \begin{bmatrix} s_{11} & s_{12} & s_{13}\\ s_{21} & s_{22} & s_{23}\\ s_{31} & s_{32} & s_{33} \end{bmatrix} \tag{19}$$

where $s_{ij}\left(i = 1,2,3; j = 1,2,3\right)$ is the element of the corresponding position of the characteristic vector matrix $\boldsymbol{S}$.

Then, Eq. (20) can be obtained from the properties of characteristic vectors.

$$\begin{bmatrix} \lambda_i - a_{11} & -a_{12} & -a_{13}\\ -a_{12} & \lambda_i - a_{22} & -a_{23}\\ 0 & 0 & \lambda_i - a_{11} \end{bmatrix}\begin{bmatrix} s_{1i}\\ s_{2i}\\ s_{3i} \end{bmatrix} = \begin{bmatrix} 0\\ 0\\ 0 \end{bmatrix} \tag{20}$$

where $i = 1, 2, 3$.

According to (20), the eigenvalue $\lambda_1, \lambda_2, \lambda_3$, eigenvector $\boldsymbol{S}_1, \boldsymbol{S}_2, \boldsymbol{S}_3$ and its matrix $\boldsymbol{S}$ corresponding to matrix $\boldsymbol{A}$ can be solved.

Since the structures of matrix $\boldsymbol{B}$ and matrix $\boldsymbol{A}$ are identical, the eigenvalue $\lambda_4, \lambda_5, \lambda_6$, the eigenvector $\boldsymbol{R}_1, \boldsymbol{R}_2, \boldsymbol{R}_3$ and the matrix $\boldsymbol{R}$ consisting of the eigenvector $\boldsymbol{R}_1, \boldsymbol{R}_2, \boldsymbol{R}_3$ can be solved by the same method.

The improved Karrenbauer transformation matrix can be obtained by contrast (10) as:

$$\boldsymbol{T} = \boldsymbol{PK}'\begin{bmatrix} \boldsymbol{S} & \boldsymbol{O}\\ \boldsymbol{O} & \boldsymbol{R} \end{bmatrix} \tag{21}$$

It can be seen from (21) that the improved Karrenbauer transformation matrix is based on the three-phase Karrenbauer transformation matrix, combined with the identical and inverse transformation matrix, and then multiplied by the corresponding characteristic vector matrix.

3 Fault location equation of untransposition double-circuit transmission line

The fault location equation of untransposed double-circuit transmission lines is based on the sinusoidal steady-state solution of the even transmission lines as shown in (9), so the voltage and current under phase measurement in (9) need to be transformed into a modulus. For untransposed double-circuit transmission lines, because of the special structure of the impedance and admittance matrices, the same modal transformation matrix cannot be used for voltage and current. The improved Karrenbauer transformation matrix $\boldsymbol{T}$ can be used as a transformation matrix for voltage, but it is not applicable for current. It can be proved that if the current transformation matrix $\boldsymbol{Q}=\boldsymbol{T}^{-T}$ is taken, the modal transformation of current can be realized. From this, the modal transformation equations of voltage and current are given as:

$$\begin{cases}\dot{\boldsymbol{U}}_{\mathrm{m}}=\boldsymbol{T}^{-1}\dot{\boldsymbol{U}}\\ \quad=\left[\dot{U}_{\mathrm{mT\alpha}}\ \dot{U}_{\mathrm{mT\beta}}\ \dot{U}_{\mathrm{mT0}}\ \dot{U}_{\mathrm{mF\alpha}}\ \dot{U}_{\mathrm{mF\beta}}\ \dot{U}_{\mathrm{mF0}}\right]^{\mathrm{T}}\\ \dot{\boldsymbol{I}}_{\mathrm{m}}=\boldsymbol{Q}^{-1}\dot{\boldsymbol{I}}\\ \quad=\left[\dot{I}_{\mathrm{mT\alpha}}\ \dot{I}_{\mathrm{mT\beta}}\ \dot{I}_{\mathrm{mT0}}\ \dot{I}_{\mathrm{mF\alpha}}\ \dot{I}_{\mathrm{mF\beta}}\ \dot{I}_{\mathrm{mF0}}\right]^{\mathrm{T}}\end{cases} \tag{22}$$

Transformation matrices $\boldsymbol{T}$ and $\boldsymbol{Q}$ can also realize the modal transformation of impedance and admittance matrices, and the transformation equation is shown as:

$$\begin{cases}\boldsymbol{Z}_{\mathrm{m}}=\boldsymbol{T}^{-1}\boldsymbol{Z}\boldsymbol{Q}\\ \quad=\mathrm{diag}\left[Z_{\mathrm{mT\alpha}}\ Z_{\mathrm{mT\beta}}\ Z_{\mathrm{mT0}}\ Z_{\mathrm{mF\alpha}}\ Z_{\mathrm{mF\beta}}\ Z_{\mathrm{mF0}}\right]\\ \boldsymbol{Y}_{\mathrm{m}}=\boldsymbol{Q}^{-1}\boldsymbol{Y}\boldsymbol{T}\\ \quad=\mathrm{diag}\left[Y_{\mathrm{mT\alpha}}\ Y_{\mathrm{mT\beta}}\ Y_{\mathrm{mT0}}\ Y_{\mathrm{mF\alpha}}\ Y_{\mathrm{mF\beta}}\ Y_{\mathrm{mF0}}\right]\end{cases} \tag{23}$$

Then, Eq. (22) is substituted into (9) to obtain the equation of even transmission lines at the modulus as:

$$\begin{cases}\frac{\mathrm{d}^2\dot{\boldsymbol{U}}_{\mathrm{m}}}{\mathrm{d}x^2}=\boldsymbol{T}^{-1}\boldsymbol{Z}\boldsymbol{Y}\boldsymbol{T}\dot{\boldsymbol{U}}_{\mathrm{m}}=\lambda\dot{\boldsymbol{U}}_{\mathrm{m}}\\ \frac{\mathrm{d}^2\dot{\boldsymbol{I}}_{\mathrm{m}}}{\mathrm{d}x^2}=\boldsymbol{Q}^{-1}\boldsymbol{Y}\boldsymbol{Z}\boldsymbol{Q}\dot{\boldsymbol{I}}_{\mathrm{m}}=\lambda\dot{\boldsymbol{I}}_{\mathrm{m}}\end{cases} \tag{24}$$

The above analysis is aimed at all sequence moduli. Since the sequence moduli are independent after decoupling, taking the identical α-sequence as an example, the fault location equation on the identical α-sequence is established. The solution of the differential equations in (24) can obtain the identical α-sequence voltage of any point f on the line as:

$$\begin{cases}\dot{U}_{\mathrm{mT\alpha.p.f}}=\dot{U}_{\mathrm{mT\alpha.p.0}}\cosh\left(\gamma_1x\right)\\ \quad-\gamma_1^{-1}Z_{\mathrm{mT\alpha}}\dot{I}_{\mathrm{mT\alpha.p.0}}\sinh\left(\gamma_1x\right)\\ \dot{U}_{\mathrm{mT\alpha.q.f}}=\left[\dot{U}_{\mathrm{mT\alpha.q.0}}\cosh\left[\gamma_1(l-x)\right]\right.\\ \quad\left.+\gamma_1^{-1}Z_{\mathrm{mT\alpha}}\dot{I}_{\mathrm{mT\alpha.q.0}}\sinh\left[\gamma_1(l-x)\right]\right]\mathrm{e}^{\mathrm{j}\delta}\end{cases} \tag{25}$$

In order to eliminate the influence of load current and improve measurement accuracy, the fault components of identical α-sequence moduli can be replaced by the identical α-sequence fault components. The fault components of p and q-terminal voltage and current modulus of untransposed double-circuit transmission lines are shown as:

$$\begin{cases}\dot{\boldsymbol{U}}_{\mathrm{m.p.0.g}}=\boldsymbol{T}^{-1}\left(\dot{\boldsymbol{U}}_{\mathrm{p.0}}-\dot{\boldsymbol{U}}_{\mathrm{p.fg.0}}\right)=\left[\dot{U}_{\mathrm{mT\alpha.p.0.g}}\ \dot{U}_{\mathrm{mT\beta.p.0.g}}\ \dot{U}_{\mathrm{mT0.p.0.g}}\ \dot{U}_{\mathrm{mF\alpha.p.0.g}}\ \dot{U}_{\mathrm{mF\beta.p.0.g}}\ \dot{U}_{\mathrm{mF0.p.0.g}}\right]^{\mathrm{T}}\\ \dot{\boldsymbol{I}}_{\mathrm{m.p.0.g}}=\boldsymbol{Q}^{-1}\left(\dot{\boldsymbol{I}}_{\mathrm{p.0}}-\dot{\boldsymbol{I}}_{\mathrm{p.fg.0}}\right)=\left[\dot{I}_{\mathrm{mT\alpha.p.0.g}}\ \dot{I}_{\mathrm{mT\beta.p.0.g}}\ \dot{I}_{\mathrm{mT0.p.0.g}}\ \dot{I}_{\mathrm{mF\alpha.p.0.g}}\ \dot{I}_{\mathrm{mF\beta.p.0.g}}\ \dot{I}_{\mathrm{mF0.p.0.g}}\right]^{\mathrm{T}}\\ \dot{\boldsymbol{U}}_{\mathrm{m.q.0.g}}=\boldsymbol{T}^{-1}\left(\dot{\boldsymbol{U}}_{\mathrm{q.0}}-\dot{\boldsymbol{U}}_{\mathrm{q.fg.0}}\right)=\left[\dot{U}_{\mathrm{mT\alpha.q.0.g}}\ \dot{U}_{\mathrm{mT\beta.q.0.g}}\ \dot{U}_{\mathrm{mT0.q.0.g}}\ \dot{U}_{\mathrm{mF\alpha.q.0.g}}\ \dot{U}_{\mathrm{mF\beta.q.0.g}}\ \dot{U}_{\mathrm{mF0.q.0.g}}\right]^{\mathrm{T}}\\ \dot{\boldsymbol{I}}_{\mathrm{m.q.0.g}}=\boldsymbol{Q}^{-1}\left(\dot{\boldsymbol{I}}_{\mathrm{q.0}}-\dot{\boldsymbol{I}}_{\mathrm{q.fg.0}}\right)=\left[\dot{I}_{\mathrm{mT\alpha.q.0.g}}\ \dot{I}_{\mathrm{mT\beta.q.0.g}}\ \dot{I}_{\mathrm{mT0.q.0.g}}\ \dot{I}_{\mathrm{mF\alpha.q.0.g}}\ \dot{I}_{\mathrm{mF\beta.q.0.g}}\ \dot{I}_{\mathrm{mF0.q.0.g}}\right]^{\mathrm{T}}\end{cases} \tag{26}$$

where $\dot{\boldsymbol{U}}_{\mathrm{p.0}}$, $\dot{\boldsymbol{I}}_{\mathrm{p.0}}$, $\dot{\boldsymbol{I}}_{\mathrm{p.0}}$ and $\dot{\boldsymbol{I}}_{\mathrm{q.0}}$ are the respective p and q terminal voltage and current of the line after a fault, while $\dot{\boldsymbol{U}}_{\mathrm{p.fg.0}}$, $\dot{\boldsymbol{I}}_{\mathrm{p.fg.0}}$, $\dot{\boldsymbol{U}}_{\mathrm{q.fg.0}}$ and $\dot{\boldsymbol{I}}_{\mathrm{q.fg.0}}$ are the voltage and current of p and q terminals of the lines before the fault (in non-fault state), respectively.

If the point f is set as the fault point, the identical α -sequence fault component in (26) is brought into (25). By replacing the identical α-sequence modulus, the identical α-sequence voltage fault component of fault point f can be obtained as:

$$\begin{cases}\dot{U}_{\mathrm{mT\alpha.p.f.g}}=\dot{U}_{\mathrm{mT\alpha.p.0.g}}\cosh\left(\gamma_1x\right)\\ \quad-\gamma_1^{-1}Z_{\mathrm{mT\alpha}}\dot{I}_{\mathrm{mT\alpha.p.0.g}}\sinh\left(\gamma_1x\right)\\ \dot{U}_{\mathrm{mT\alpha.q.f.g}}=\left[\dot{U}_{\mathrm{mT\alpha.q.0.g}}\cosh\left[\gamma_1(l-x)\right]\right.\\ \quad\left.+\gamma_1^{-1}Z_{\mathrm{mT\alpha}}\dot{I}_{\mathrm{mT\alpha.q.0.g}}\sinh\left[\gamma_1(l-x)\right]\right]\mathrm{e}^{\mathrm{j}\delta}\end{cases} \tag{27}$$

Then, Eqs. (25)–(27) are all established under the identical α sequence component. For other sequences, since sequence components are independent of each other and the structures of sequence parameters and variables are similar, the same method can be used to obtain the identical β-sequence voltage fault components $\dot{U}_{\mathrm{mT\beta.p.f.g}}$ and $\dot{U}_{\mathrm{mT\beta.q.f.g}}$, the identical zero-sequence voltage fault components $\dot{U}_{\mathrm{mT0.p.f.g}}$ and $\dot{U}_{\mathrm{mT0.q.f.g}}$, the inverse α-sequence voltage fault components $\dot{U}_{\mathrm{mF\alpha.p.f.g}}$ and $\dot{U}_{\mathrm{mF\alpha.q.f.g}}$, the inverse β-sequence voltage fault components $\dot{U}_{\mathrm{mF\beta.p.f.g}}$ and $\dot{U}_{\mathrm{mF\beta.q.f.g}}$, and the inverse zero-sequence voltage fault component $\dot{U}_{\mathrm{mF0.p.f.g}}$ and $\dot{U}_{\mathrm{mF0.q.f.g}}$ of the fault point f.

In addition to the load current, the influence of sampling asynchronous angle and parameter asymmetry caused by untransposition on each sequence component will affect location accuracy, and thus needs to be eliminated when establishing the location equation. Because the asynchronous angle δ of data sampling only affects the phase of each sequence voltage fault component at fault point f without affecting the magnitude, the equation is established by using the magnitude of voltage fault component. The different influence degree of parameter asymmetry on each sequence component will directly lead to a different error size of location with different sequence components. If only a single sequence component is used for location, there will be error fluctuation. Therefore, all six sequence components are used to establish the location process, and then the results of each equation are averaged.

4 Solution of location equation based on QPSO

After analyzing the main influencing factors of location accuracy, using the principle that the magnitude of each sequence voltage fault component of fault point f deduced from the p terminal is equal to that of each sequence voltage fault component of fault point f deduced from the q terminal, the distance measurement equation is established as:

$$\begin{cases} f_1(x_1) = \left| \left| \dot{U}_{\mathrm{mT\alpha.p.f.g}}(x_1) \right| - \left| \dot{U}_{\mathrm{mT\alpha.q.f.g}}(x_1) \right| \right| \\ f_2(x_2) = \left| \left| \dot{U}_{\mathrm{mT\beta.p.f.g}}(x_2) \right| - \left| \dot{U}_{\mathrm{mT\beta.q.f.g}}(x_2) \right| \right| \\ f_3(x_3) = \left| \left| \dot{U}_{\mathrm{mT0.p.f.g}}(x_3) \right| - \left| \dot{U}_{\mathrm{mT0.q.f.g}}(x_3) \right| \right| \\ f_4(x_4) = \left| \left| \dot{U}_{\mathrm{mF\alpha.p.f.g}}(x_4) \right| - \left| \dot{U}_{\mathrm{mF\alpha.q.f.g}}(x_4) \right| \right| \\ f_5(x_5) = \left| \left| \dot{U}_{\mathrm{mF\beta.p.f.g}}(x_5) \right| - \left| \dot{U}_{\mathrm{mF\beta.q.f.g}}(x_5) \right| \right| \\ f_6(x_6) = \left| \left| \dot{U}_{\mathrm{mF0.p.f.g}}(x_6) \right| - \left| \dot{U}_{\mathrm{mF0.q.f.g}}(x_6) \right| \right| \end{cases} \tag{28}$$

$$F(x_1, x_2, x_3, x_4, x_5, x_6) = \sum_{i=1}^{6} f_i(x_i) = 0 \tag{29}$$

where $x_1, x_2, x_3, x_4, x_5, x_6$ are the distances from the p-terminal of the line to the fault point f under each sequence component, respectively.

Considering that (29) is a transcendental equation composed of hyperbolic functions with multi-dimensional complex variables, the exact analytical solution cannot be obtained, and the approximate solution satisfying the accuracy can only be obtained by an iterative method. However, power system fault location requires a fast location speed while satisfying the location accuracy, otherwise it can affect the action and effect of relay protection devices. Therefore, the relevant iterative algorithms should have short iteration time and fast iteration speed while meeting the requirements of high accuracy. For the improved iterative algorithms such as gradient descent method and quasi Newton method commonly used in power system analysis, although the accuracy of the final solution is improved, the number and speed of iterations are also affected. For ant colony, genetic, particle swarm optimization (PSO) and other algorithms, there are problems such as too many iterations and that it is easy for them to fall into local optima.

Compared with traditional PSO algorithm, QPSO algorithm introduces quantum theory as its basis, which means that the QPSO algorithm retains the advantages of PSO algorithm but offers further improvement. Its advantages are mainly: first, the QPSO algorithm only has a displacement model, so only the particle positions need to be updated in the iteration process, while the PSO algorithm has speed and displacement models, so the positions and speeds of particles need to be updated simultaneously in the iteration process. Therefore, the QPSO algorithm has higher iteration efficiency. Secondly, for the QPSO algorithm, the particles in the quantum system do not move with the determined trajectory and their positions are distributed at any point in the solution space with a certain probability. Therefore, they have the ability of global search and can effectively avoid falling into the problem of local optima. Finally, the QPSO algorithm has fewer control parameters than genetic and PSO algorithms. This, is convenient for its application in practical problems.

4.1 Mathematical model of QPSO

For the PSO algorithm, if every particle can converge to a local attraction, then PSO may converge. Each dimension of the local attraction is given as:

$$p_{id}(t) = \varphi_d(t) P_{id}(t) + [1 - \varphi_d(t)] P_{gd}(t) \tag{30}$$

where t is the current time of iterations, D is the particle dimension, and $\varphi_d(t)$ is a random number evenly distributed on $(0, 1)$. $P_i(t)$ is the individual optimum position of the ith particle, and $P_g(t)$ is the best position for the group.

In quantum space, the particle state is determined by the wave function ψ and the probability density function of the particle position is $|\psi|^2$. For non-rotating particles, the state depends on the wave function and is position dependent only. Assuming that the particle is in a potential well and the center of the potential well is a local attraction, the potential well of the particle in dimension d is $p_{id}(t)$. In a potential well, the further the particle is from the center of the potential well, the closer the wave function ψ approaches 0, i.e., the probability of particle occurrence is small. The closer the particle is to the potential well, the closer its kinetic energy E approaches 0, making it impossible for the particle to escape. Therefore, the wave function of the ith particle can be obtained at the $(t+1)$th iteration as:

$$\psi[x_{id}(t+1)] = \frac{\exp\left[-\frac{|x_{id}(t+1) - p_{id}(t)|}{L_{id}(t)}\right]}{\sqrt{L_{id}(t)}} \tag{31}$$

where $L_{id}(t)$ is the standard deviation of the biexponential distribution, representing the potential well length, and $x_{id}(t+1)$ is the particle position at the $(t+1)$th iteration.

The probability density function Q and probability distribution function T of particles can be obtained respectively as:

$$Q[x_{id}(t+1)] = |\psi[x_{id}(t+1)]|^2 = \frac{1}{L_{id}(t)} \exp\left[-\frac{2|x_{id}(t+1) - p_{id}(t)|}{L_{id}(t)}\right] \tag{32}$$

$$T[x_{id}(t+1)] = \exp\left[-\frac{2|x_{id}(t+1) - p_{id}(t)|}{L_{id}(t)}\right] \tag{33}$$

Based on the particle wave function ψ, probability density function Q and probability distribution function T, the particle position update obtained by the Monte Carlo method is given as:

$$x_{id}(t+1) = p_{id}(t) \pm \frac{L_{id}(t)}{2} \ln\left[\frac{1}{u_{id}(t)}\right] \tag{34}$$

where $u_{id}(t)$ is a random number evenly distributed over (0, 1).

The value of $L_{id}(t)$ can be determined by:

$$L_{id}(t) = 2\alpha|m_{\text{best}}(t) - x_{id}(t)| \tag{35}$$

where α is the control parameter, called compression-expansion factor. $m_{\text{best}}(t)$ is the average of the individual optimum position of each dimension of the particle at the tth iteration. This is called the average optimum position.

The value of $m_{\text{best}}(t)$ can be determined by:

$$m_{\text{best}}(t) = \frac{1}{N}\sum_{i=1}^{N} P_i(t) \tag{36}$$

where N is the number of particles.

The updating equations of particle positions obtained from (35) and (36) are shown as:

$$x_{id}(t+1) = p_{id}(t) \pm \alpha|m_{\text{best}}(t) - x_{id}(t)| \ln\left[\frac{1}{u_{id}(t)}\right] \tag{37}$$

The updating method of the individual optimum position $P_i(t)$ and the group optimum position $P_g(t)$ of the particles is identical to that of the PSO algorithm, and the updating equations are shown as:

$$P_i(t+1) = \begin{cases} x_i(t+1) & ,f[x_i(t+1)] < f[P_i(t)] \\ P_i(t) & ,f[x_i(t+1)] \geq f[P_i(t)] \end{cases} \tag{38}$$

$$P_g(t+1) = \arg\min_{1 \leq i \leq N} \{f[P_i(t)]\} \tag{39}$$

where $f()$ is the fitness function.

It should be noted that, as the only control parameter α, except the number of particles, particle dimension and iteration time, it can be set with fixed value, linear reduction, or other strategies. In [22], the characteristics and performance of these three strategies are compared and combined with the simulation results of standard test functions, and a practical and instructive control parameter selection method is given. This selection method points out that the fixed value strategy has a large standard deviation and poor robustness, while compared with the nonlinear reduction strategy, the linear reduction strategy can get better results in most cases. Therefore, in this paper, the linear reduction strategy is adopted, and its setting equation is shown as:

$$\alpha = 1 - \frac{1}{2}\frac{t}{t_{\max}} \tag{40}$$

where $t_{\max}$ is the maximum number of iterations.

4.2 Optimum solution of location equation

Assuming the total length of untransposed double-circuit transmission lines is l, the fitness function of the algorithm is the fault location equation shown in (29). The flow chart of the QPSO algorithm is shown in Fig. 3 and

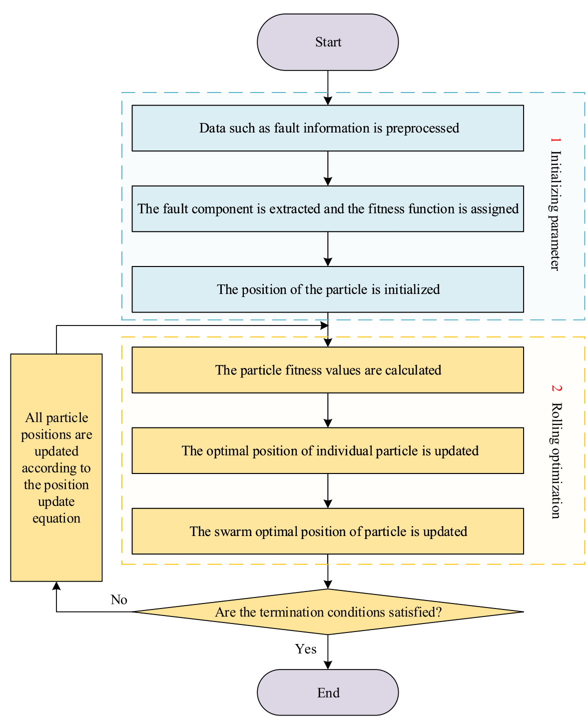

Fig. 3 Flow chart of the QPSO algorithm

the algorithm steps for optimizing the distance measurement equation are:

1. Initialize particle position in each six-dimensional space with a one-dimensional range $[0, l]$.
2. According to the initial position of the particle, the fitness function corresponding to the initial position of the particle is calculated to initialize the individual optimum position P_i and the group optimum position P_g of the particle.
3. Update the average optimum position of particles according to (36) and update the position of particles according to (37).
4. Calculate the current fitness function value according to the current position of the particle and compare it with the fitness function value of the previous iteration. If the current fitness function value is less than the fitness function value corresponding to the individual optimum position in the previous iteration (i.e., $f[x_i(t+1)] < f[P_i(t)]$), the particle position is updated to the individual optimum position $(P_i(t+1) = x_i(t+1))$.
5. Update the group optimum position $P_g(t+1)$ according to (38), compare the fitness function value corresponding to the current group optimum position with the fitness function value corresponding to the group optimum position at the previous iteration. Update it to the group optimum position if the fitness function value corresponding to the current group optimum position is small.
6. Repeat steps 3 to 5 until the number of iterations reaches the set maximum number of iterations.

At the end of the iteration, the optimal group position P_g is the result of the optimization of the location function, and each dimension value of P_g is the obtained fault distance. In order to reduce error fluctuation, the final fault distance is obtained by averaging the six-dimensional results.

5 Results and discussion

In PSCAD, the model of untransposed double-circuit transmission lines shown in Fig. 1 is established, and relevant programs are programmed in MATLAB to realize modal transformation of parameters and fault location based on the QPSO algorithm. In the model, the voltage level of the double-circuit lines is 220 kV, the positive impedance of the power supply at both ends is $Z_{\mathrm{M1}} = 3.39 + \mathrm{j}49.34\Omega$, the zero-sequence impedance is $Z_{\mathrm{M0}} = 2.52 + \mathrm{j}46.03\Omega$, and the phase of the power supply at the sending end is 15 degrees ahead of the receiving end. A Frequency-Dependent (Phase) model is used for the overhead lines, while untransposition mode is selected for all the overhead lines. The length of the lines is 200 km, and the specific parameters are shown in Table 1.

Table 1 Overhead line parameters

Type	Parameter	Value
Tower parameters	Ground height of the lowest conductor (m)	24
	Horizontal distance between inner conductors (m)	5.5
	Horizontal distance between inner and outer conductors of single circuit line (m)	6
	Vertical distance between upper and lower conductors of single circuit line (m)	7.5
	Vertical distance between ground wire and the lowest conductor (m)	9.5
	Distance between two ground wires (m)	14
Wire parameters	Outer radius of conductor (m)	0.01341
	Radius of single strand (m)	0.0032
	Number of strands in total	55
	Conductor DC Resistance (Ω km^{-1})	0.07389
	Wire splitting number	2
	Wire split spacing (m)	0.4

Table 2 Decoupled parameters of each sequence impedance and admittance

Line parameters	Identical α sequence components (Ω)	Identical β sequence components (Ω)	Identical 0 sequence components (Ω)	Inverse α sequence components (Ω)	Inverse β sequence components (Ω)	Inverse 0 sequence components (Ω)
Impedance (10^{-2})	0.2665 + j2.5809	9.6843 + j30.599	0.4118 + 3.2193j	− 0.7019 + 1.4024j	− 1.8141 + 3.7724j	0.4123 + 2.9974j
Admittance (10^{-5})	0.0177 + j4.4509	0.0117 + j1.0028	0.0090 + 3.4694j	4.0357 + 6.1075j	1.6139 + 2.4050j	0.0090 + 3.7764j

Table 3 Comparison results of eigenvalues

Computing method	λ_1	λ_2	λ_3	λ_4	λ_5	λ_6
Matlab (10^{-12})	− 1.1483 + 0.1232j	− 3.0574 + 1.0070j	− 1.1165 + 0.1457j	− 1.1398 + 0.1372j	− 1.2000 + 0.1725j	− 1.1316 + 0.1584j
Paper method (10^{-12})	− 1.1483 + 0.1232j	− 3.0574 + 1.0070j	− 1.1165 + 0.1457j	− 1.1398 + 0.1372j	− 1.2000 + 0.1725j	− 1.1316 + 0.1584j

5.1 Simulation verification of modal conversion

In order to fully verify the accuracy and reliability of this method, the modal transformation between impedance matrix $\boldsymbol{Z}$ and admittance matrix $\boldsymbol{Y}$ of the untransposed double-circuit transmission lines obtained by PSCAD simulation is carried out by the improved Karrenbauer matrix. The decoupled impedance and admittance parameters are shown in Table 2. Then the eigenvalues obtained by decoupling the impedance and the admittance product matrix $\boldsymbol{ZY}$ with the improved Karrenbauer matrix are compared with the precise results calculated by the MATLAB mathematical toolkit, and the comparison of results is shown in Table 3.

From Tables 2 and 3, it can be seen that the improved Karrenbauer matrix proposed in this paper can effectively and accurately transform impedance matrix $\boldsymbol{Z}$ and admittance matrix $\boldsymbol{Y}$. Compared with the accurate results calculated by MATLAB mathematical toolkit, the error is very small.

It should be noted that, although the mathematical meaning of $\boldsymbol{\lambda}$ in (10) is the eigenvalue matrix, from the perspective of modal transformation, $\boldsymbol{\lambda}$ in (24) is the product of sequence impedance and admittance under the decoupled modal parameter. It has similar meaning to the product of positive, negative and zero sequence impedance admittance in Fortescue's transformation method, but also has essential differences. It can be seen from Table 2 that, as the product of sequence impedance and admittance under the decoupled modal parameter, the product modal (sequence) components of each sequence impedance and admittance in $\boldsymbol{\lambda}$ are not equal to each other, which is completely different from Fortescue's transformation method. The impedance and admittance of the positive sequence and negative sequence after decoupling are equal to each other in Fortescue's method. Therefore, the six sequence components method or other modal transformation method based on Fortescue's method is not applicable for the untransposed double-circuit transmission lines.

It should also be noted that the real component of inverse α-sequence and β-sequence impedances in Table 2 are negative. Although matrix $\boldsymbol{P}$ can decompose the six phases of the untransposition double-circuit transmission lines, because of the asymmetry caused by the untransposition, the decomposition results are no longer the identical and inverse vectors in the component sense. Therefore, the inverse α-sequence and β-sequence impedances with negative real components are not of practical physical significance, but only participate in the establishment of fault location equation as an intermediate process.

5.2 Fault location simulation verification

In order to verify the practical effect of the improved Karrenbauer matrix and QPSO algorithm in fault location of untransposed double-circuit transmission lines, different fault distances and types of faults with different grounding resistances are simulated and verified. Although its probability of occurrence is low, a cross-line fault is still a unique fault type of the double-circuit lines, and has important research value because of the electromagnetic coupling and power injection between the double-circuit transmission lines. Therefore, this paper carries out simulation verification for single-circuit line faults and double-circuit cross-line faults. The definition of relative fault location error ξ is:

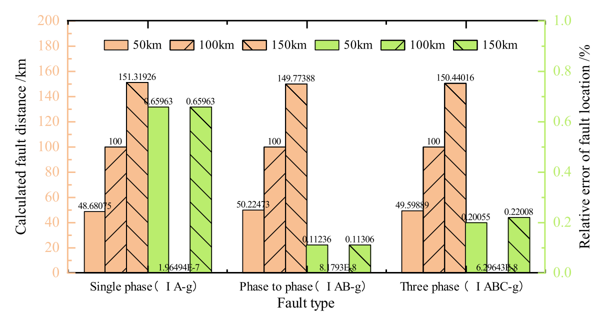

Fig. 4 Fault location results of different types of single-circuit line faults when the transition resistance is 0.01 Ω

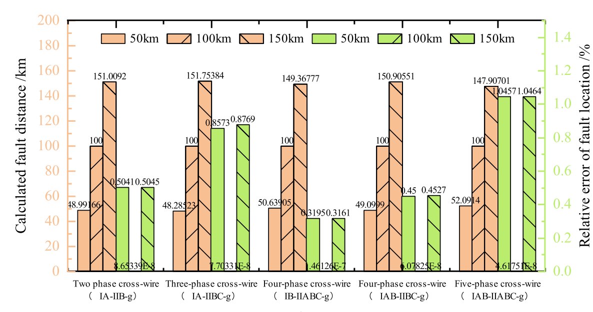

Fig. 5 Fault location results of different types of cross-line faults when the transition resistance is 0.01 Ω

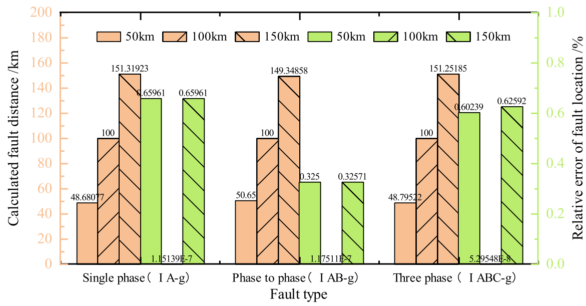

Fig. 6 Fault location results of different types of single-circuit line faults when the transition resistance is 50 Ω

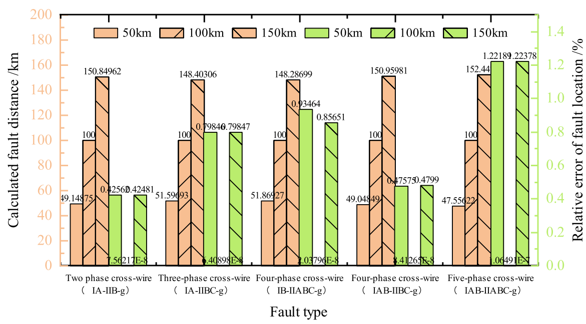

Fig. 7 Fault location results of different types of cross-line faults when the transition resistance is 50 Ω

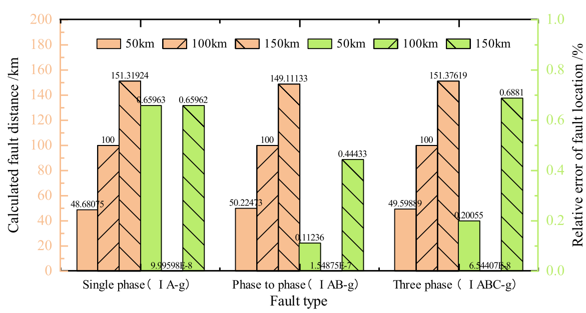

Fig. 8 Fault location results of different types of single circuit line fault when transition resistance is 100 Ω

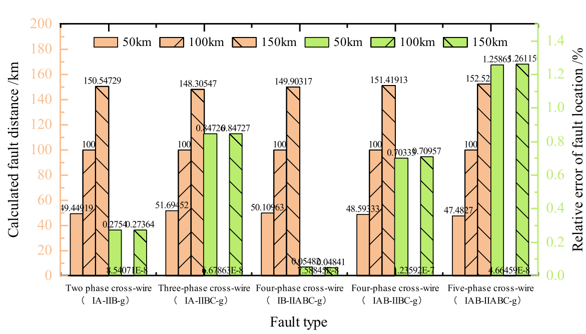

Fig. 9 Fault location results of different types of cross line fault when transition resistance is 100 Ω

$$\xi = \left| \frac{l_{ca} - l_{re}}{l} \right| \times 100\% \tag{41}$$

where l_{ca} is the calculated fault distance, and l_{re} is the actual fault distance.

Figures 4 and 5 give the location results for different types of single-circuit faults and double-circuit cross-line faults, respectively, at different fault distances when the ground resistance (0.01 Ω) is small. From the location errors, it can be seen that the location errors meet the engineering requirements for single-circuit and double-circuit cross-line faults.

Figures 6 and 7 give the respective results of fault location for different types of single-circuit and double-circuit cross-line faults at different fault distances when the ground resistance is 50 Ω. By comparing the results with those in Figs. 4 and 5, it can be seen that the location errors are also small and do not change with the change of ground resistance.

Figures 8 and 9 give the location results for different types of single-circuit and double-circuit cross-line faults, respectively, at different fault distances when the ground resistance (100 Ω) is high. It can be seen that when there is high resistance grounding, the results of fault location also meet the requirements and are not affected by the fault types and fault distances.

Figures 4, 5, 6, 7, 8 and 9 show that the results of fault location are not affected by ground resistance, and regardless of the ground resistance value, the location results can always reach a high accuracy.

5.3 Comparison with other ranging methods

In order to verify the superior performance and high accuracy of the proposed fault location method based on the improved Karenbauer matrix and QPSO algorithm, the simulation results are compared with the results of other fault location methods. Reference [23] aims at the coupling parameter matrix of untransposed double-circuit transmission lines, and by constructing the perturbation of the impedance matrix of untransposed double-circuit transmission lines, the eigenvalues and eigenvectors of the impedance matrix of the line are separately expanded by the perturbation method, and the modal transformation matrix of different precision is obtained through the equations satisfying different orders. The obtained transformation matrix is then applied to fault location based on modulus component theory. The results obtained by the fault location method in [23] are compared with those obtained by the proposed method, as shown in Table 4.

It can be seen from Table 4 that the proposed method of fault location for untransposed double-circuit transmission lines based on the improved Karenbauer matrix

Table 4 Comparison of two location methods

Fault type	Fault location error with the proposed method (%)	Fault location error with the method in [22] (In the case of the zero order) (%)
Single phase ground fault (A-g)	0.6596	1.7527
Two-phase ground fault (AB-g)	0.1123	1.1441
Three phase ground fault (ABC-g)	0.2005	4.0004

and QPSO algorithm has superior performance and higher accuracy than those from [23], and thus it can be well applied to engineering practice.

5.4 Discussion

From the analysis of Figs. 4, 5, 6, 7, 8 and 9, it can be seen that the methods proposed in this paper are not affected by the common influencing factors of location accuracy, such as fault type, fault distance and ground resistance. With different fault types, fault distances and ground resistances, this method can achieve high accuracy fault location for untransposed double-circuit transmission lines.

For the faults with different ground resistances and different fault types with fault distance of 100 km, the error is significantly smaller and the relative error is close to zero compared with the faults with other fault distances under the same conditions. There are two reasons for this. First, the fault point is located at the middle of the line and the voltage and current measured at both ends of the line are relatively symmetrical, which reduces the error caused by the decomposition of the identical and inverse transformation matrix $\boldsymbol{P}$. On the other hand, the QPSO algorithm used in this paper has high performance and can get high accuracy results with fewer iterations and higher iteration speed.

The QPSO technique will produce different results if the same model is run a number of times, which influences the accuracy of the location results. However, because of the high performance of QPSO, the difference between the results of each calculation is very small, and the impact on the accuracy of fault location results can thus be ignored.

It should also be pointed out that, because of the good performance of the QPSO algorithm, the fault location equations of all fault types have converged at the 100th iteration when the QPSO algorithm is used to optimize the solution. Therefore, the maximum number of iterations in the QPSO algorithm is set to 100, and it can be seen from the simulation results that the obtained fault location error meets the accuracy requirements. As for location speed, because of the excellent search performance and the simplification of the iterative model of the QPSO algorithm, the iterative process takes little time and has little impact on location speed. Taking the single-phase ground fault location with transition resistance of 0.01 Ω and fault distance of 50 km as an example, it can be concluded through multiple simulations that when the maximum iteration number is set to 100, the time of running the iteration process is between 0.0787 and 0.0938 s due to the randomness of particle occurrence position. Therefore, the time spent in the iterative process has little impact on the speed of fault location.

6 Conclusion

In this paper, a new method for fault location of untransposed double-circuit transmission lines based on an improved Karrenbauer matrix and QPSO algorithm is proposed. The three-phase Karrenbauer matrix is improved and the identical and inverse component transformation is introduced to obtain a matrix suitable for modal transformation of untransposed double-circuit transmission lines. According to the characteristics of six-sequence parameters after decoupling, a fault location equation based on two-terminal electrical quantities is established, and the QPSO algorithm is introduced to optimize the solution of the equation and carry out simulation verification. Through the analysis of relevant results and errors, the conclusions are:

1. For untransposed double-circuit transmission lines, when single-circuit and double-circuit cross-line faults of different fault types occur at any point of the lines, regardless of the ground resistance, the modal transformation and the location equation and its algorithm proposed in this paper can be used for fault location. Furthermore, since the fault location equation in this paper is based on a sinusoidal steady fault component, the fault inception angle has no influence on the accuracy of fault location. The results of fault location have high accuracy and can well meet the requirements of engineering practice.
2. For untransposed double-circuit transmission lines, because of the asymmetry of impedance and admittance parameters and mutual inductance between lines, the impedance and admittance components of positive and negative sequence after decoupling are no longer equal. If the traditional Fortescue's transformation method or other modal transformation method based on complete transposition assumption were to be used, large errors would occur, which could affect the accuracy of location.

3. As an important tool for modal transformation, the Karrenbauer matrix is widely used in relay protection devices because of its simple structure. The method proposed in this paper is based on a three-phase Karrenbauer matrix. Therefore, in practical application, the basic principle of relevant relay protection devices need not be changed, while only the corresponding improvements are needed according to line parameters, so the proposed method has good applicability.

The method proposed in this paper has high location accuracy and is applicable to fault location of all types of faults of untransposed double-circuit transmission lines. It has good engineering application value. The location principle and the method of the relay protection device for untransposition double-circuit transmission lines can be adjusted according to this method to ensure that the relay protection device can accurately realize fault location in the event of various types of faults.

Abbreviations

QPSO Quantum-behaved particle swarm optimization
PSCAD Power system computer aided design

Acknowledgements

This work was sponsored by the National Natural Science Foundation of China (No. 62363022, 61663021, 71763025, 61861025), and the Natural Science Foundation of Gansu Province (No. 23JRRA886), and the Gansu Provincial Department of Education: Industrial Support Plan Project (No. 2023CYZC-35). Their support is greatly appreciated.

Authors' information

M. A. Tang (1973–), male, Ph.D. and Professor, Major in the analysis of electric power system and power system protection and control.
H. Lu (1995–), male, postgraduate, the main research direction is the analysis of electric power system.
B. Li (1976–), male, Ph.D. and Professor, Major in the protection and control of power systems and microgrids.

Author contributions

All authors contributed to the study conception and commented on previous versions of the manuscript. The individual contributions of the authors are specified as follows: MT: Conceptualization, Methodology, Supervision, Writing-Reviewing and Editing, Funding Acquisition. HL: Conceptualization, Methodology, Software, Writing-original draft. BL: Technical Guidance, Original Conception. All authors read and approved the final manuscript.

Funding

This research was funded by the National Natural Science Foundation of China (No. 62363022, 61663021, 71763025, 61861025), and the Natural Science Foundation of Gansu Province (No. 23JRRA886), and the Gansu Provincial Department of Education: Industrial Support Plan Project (No. 2023CYZC-35).

Availability of data and materials

The datasets used and/or analysed during the current study are available from the corresponding author on reasonable request.

Declarations

Competing interests

The authors declare that they have no known competing financial interests or personal relationships that could have appeared to influence the work reported in this paper.

Author details

[1]School of New Energy and Power Engineering, Lanzhou Jiaotong University, Lanzhou, China. [2]School of Electrical and Information Engineering, Tianjin University, Tianjin, China.

Received: 27 October 2022 Accepted: 23 August 2023
Published online: 13 September 2023

References

1. Xi, J., Wu, W., & Wu, S. (2011). New methods of analysis of the unbalanced degree of the transmission line based on Thevenin equivalent. *Power System Protection and Control, 39*(21), 7–11.
2. Kang, N., & Liao, Y. (2012). Double-circuit transmission line fault location with the availability of limited voltage measurements. *IEEE Transactions on Power Delivery, 27*(1), 325–336.
3. Zhu, Q., Liu, Q., Chen, H., Luo, L., He, D., Wei, S., Zeng, F., & Hua, H. (2014). Study on voltage imbalance of un-transposed double-circuit lines on the same tower. *Power System Protection and Control, 42*(07), 73–79.
4. Ren, P. X., Ler-Ari, H., & Abur, A. (2018). Tracking three-phase untransposed transmission line parameters using synchronized measurements. *IEEE Transactions on Power Systems, 33*(4), 4155–4163.
5. Vieira, D. A. G., Oliveira, D. B., & Lisboa, A. C. (2013). A closed-form solution for untransposed transmission-lines fault location with nonsynchronized terminals. *IEEE Transactions on Power Delivery, 28*(1), 524–525.
6. Li, B., Guo, F. R., Li, X., & Bo, Z. B. (2014). Circulating unbalanced currents of EHV/UHV untransposed double-circuit lines and their influence on pilot protection. *IEEE Transactions on Power Delivery, 29*(2), 825–833.
7. Lu, D., Liu, Y., Chen, S., Wang, B. L., & Lu, D. Y. (2022). An improved noniterative parameter-free fault location method on untransposed transmission lines using multi-section models. *IEEE Transactions on Power Delivery, 37*(3), 1356–1369.
8. Ge, Y. (2007). *Principle and technology of new relay protection and fault location* (2nd ed.). Xi'an Jiaotong University Press.
9. Li, Y., Huang, S., Xu, Z., & Zhang, Y. (2010). Research of individual phase modeling of un-transposed high voltage transmission lines and analysis of its unbalanced operation. *Automation of Electric Power Systems, 34*(19), 75–80.
10. Jiang, T., Guo, Z., Chen, X., & Bai, X. (2002). Polymorphic phase components method and its application in three-phase unbalance calculation of power system. *Proceedings of the CSEE, 22*(05), 71–75.
11. Wang, A., Chen, Q., & Zhou, Z. (2008). An improved phase components method for arbitrary complicated power system fault analysis. *Automation of Electric Power Systems, 32*(18), 39–43.
12. Dobakhshari, A. S. (2017). Noniterative parameter-free fault location on untransposed single-circuit transmission lines. *IEEE Transactions on Power Delivery, 32*(3), 1636–1644.
13. Jia, P., Zhang, Q., Jia, X., & Wei, C. (2013). Clarke matrix based solution of phase-mode transformation matrix of asymmetrical transmission lines. *Power System Technology, 37*(09), 2653–2657.
14. Faria, J. A. B., & Mendez, J. H. B. (1997). Modal analysis of untransposed bilateral three-phase lines: A perturbation approach. *IEEE Transactions on Power Delivery, 12*(1), 497–504.
15. Brandao, F. J., & Hildemaro, B. J. (1997). On the modal analysis of asymmetrical three-phase transmission lines using standard transformation matrices. *IEEE Transactions on Power Delivery, 12*(4), 1760–1765.
16. Wang, P., Song, J., Liang, F., et al. (2021). Equivalent model of multi-type distributed generators under faults with fast-iterative calculation method based on improved PSO algorithm. *Protection and Control of Modern Power Systems, 29*(6), 1–12.
17. Wu, B., Yu, Z., Zou, H., & Tai, N. (2015). Fault location for four-parallel transmission lines on same tower based on ant colony algorithm. *Power System Protection and Control, 43*(20), 45–50.
18. Wu, X. M., Wang, D. H., Cao, W. H., & Ding, M. (2019). A genetic-algorithm support vector machine and D-S evidence theory based fault diagnostic model for transmission line. *IEEE Transactions on Power Delivery, 33*(6), 4186–4194.
19. Jamali, S., Bahmanyar, A., & Ranjbar, S. (2020). Hybrid classifier for fault location in active distribution networks. *Protection and Control of Modern Power Systems, 17*(5), 1–9.

20. Asadi Majd, A., Samet, H., & Ghanbari, T. (2017). k-NN based fault detection and classification methods for power transmission systems. *Protection and Control of Modern Power Systems, 32*(2), 1–11.
21. Mikki, S. M., & Kishk, A. A. (2006). Quantum particle swarm optimization for electromagnetics. *IEEE Transactions on Antennas and Propagation, 54*(10), 2764–2775.
22. Fang, W., Sun, J., Xie, Z., & Xu, W. (2010). Convergence analysis of quantum-behaved particle swarm optimization algorithm and study on its control parameter. *Acta Physica Sinica, 59*(06), 3686–3694.
23. Zhang, Q., Yi, L., Wang, D., et al. (2018). Application of perturbation method to un-transposed double-circuit transmission lines. *Proceedings of the CSU-EPSA, 30*(7), 110–116.